New Classes of Miniaturized Planar Marchand Baluns

Wael M. Fathelbab, *Member, IEEE,* and Michael B. Steer, *Fellow, IEEE*

***Abstract*—Three new classes of miniaturized Marchand balun are defined based on the synthesis of filter prototypes. They are suitable for mixed lumped-distributed planar realizations with small size resulting from transmission-line resonators being a quarter-wavelength long at frequencies higher than the passband center frequency. Each class corresponds to an S-plane bandpass prototype derived from the specification of transmission zero locations. A tunable 50 : 100-Ω balun is realized at 1 GHz to demonstrate the advantages of the approach presented here.**

***Index Terms*—High-pass/bandpass prototypes, Marchand balun, network synthesis, transmission zeros.**

I. Introduction

EXACT synthesis of filters with prescribed transfer functions has been pursued for several decades and has led to a wealth of different classes of prototypes satisfying the stringent requirements of communication systems. These synthesis techniques have been successfully used to design low-pass, high-pass, bandpass, and bandstop filters with excellent electrical performance. To a limited extent, this network synthesis approach has been applied to the design of the Marchand balun [1]. This includes an implementation of the coaxial transmission-line Marchand balun [2] and its corresponding planar coupled-line form [3]. In both approaches, the balun design was based on an S-plane high-pass prototype using the Richards' transformation $S = j\tan(\pi/2(f/f_o))$, where f and S are the real and complex frequency variables, respectively, and f_o is the center frequency of the passband. Upon synthesis of such a prototype, the coupled-line parameters of the Marchand balun may then be computed [2]. The high-pass prototype becomes a periodic bandpass in the frequency plane (f-plane) with the first passband centered at f_o. A planar Marchand balun of this type and its corresponding equivalent circuit are shown in Fig. 1. The drawback of such a design is that the center frequency of the balun is actually the resonant frequency of the transmission-line resonators forming the balun. In other words, the overall size of a conventional Marchand balun is determined by its center frequency. This limits the use of the S-plane high-pass prototype in situations where small size is critical such as in systems operating at low frequencies. The focus of this paper is the miniaturization of the Marchand balun, and this requires that the balun's center frequency f_o and the quarter-wave frequency f_q of the transmission-line resonators be different. To permit independent specification of f_o and f_q, an S-plane bandpass prototype must be synthesized so that in the f-plane a periodic bandpass behavior is achieved. This basic idea was used to design a planar lumped-distributed transmission-line balun [4] that consisted of a power divider and a pair of bandpass phase shifters. Now Richards' transformation becomes $S = j\tan(\pi/2(f/f_q))$ with f_q chosen to be above the passband centered at f_o. Here, f_q is also referred to as the commensurate frequency. Hence, a balun design based on a suitable S-plane bandpass prototype will feature reduction in its overall size.

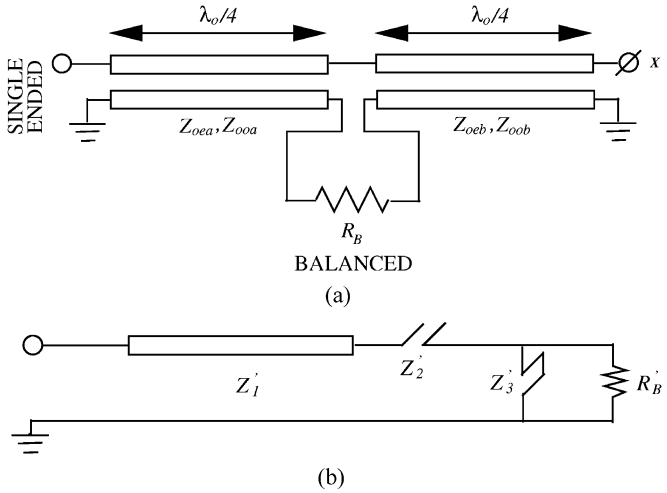

Fig. 1. Conventional Marchand balun. (a) Physical layout with balanced load impedance R_B. (b) S-plane high-pass prototype.

In [5], a semilumped balun was implemented but without design theory. More recently, derivation of analytic formulas for a class of lumped-distributed baluns led to useful design charts, but the approach lacks generality [6]. Another key design parameter in balun design is bandwidth, which is thoroughly investigated in [3] with a conclusion that requires multilayer coupled-line realizations as presented in [7]–[9].

In this paper, the design of baluns corresponding to bandpass prototypes in the S-plane is investigated. This synthesis approach provides design insight and only requires minimum circuit optimization. The reason for this is that the specified transfer function is decomposed into its constituents, i.e., the elements of the synthesized prototype, thus enabling control of all available design parameters. Aided by the use of appropriate circuit transformations, novel balun topologies can be created that achieve performances as close as possible to the theoretical maximum in terms of size and bandwidth.

Section II describes the derivation of an S-plane bandpass balun leading to simple analytic expressions for quick reference. In Section III, the new S-plane bandpass baluns are classified in

Manuscript received May 8, 2004; revised October 5, 2004. This work was supported by the U.S. Army Research Office as a Multidisciplinary University Research Initiative on Multifunctional Adaptive Radio Radar and Sensors under Grant DAAD19-01-1-0496.

The authors are with the Department of Electrical and Computer Engineering, North Carolina State University, Raleigh, NC 27695-7911 USA (e-mail: wmfathel@ncsu.edu).

Digital Object Identifier 10.1109/TMTT.2005.845707

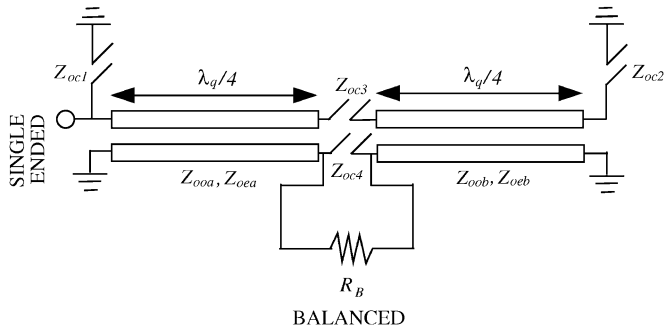

Fig. 2. S-plane bandpass Marchand balun with balanced load impedance R_B.

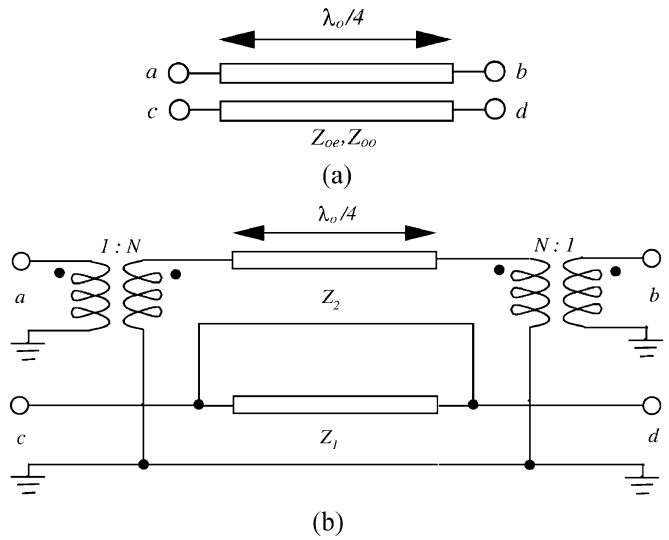

Fig. 3. Pair of symmetrical coupled-lines in homogenous media from [10]. (a) Physical layout. (b) Equivalent network model.

terms of their prototypes, and in Section IV a detailed numerical design example is presented. Finally, the balun of the numerical example is implemented and its measured characteristics reported. Also, the center frequency of the implemented balun is tuned using varactor diodes to suit wide-band applications.

II. Derivation of a Bandpass Marchand Balun

The focus of this section is demonstrating that the procedure of element extraction from a chosen prototype corresponds to the most general bandpass balun topology. By appropriately loading the high-pass balun of Fig. 1(a) with open-circuited stubs, the bandpass balun of Fig. 2 results. The equivalent prototype of this structure can be derived in an identical fashion to that in [3] by utilizing the network model of a pair of coupled lines in homogeneous media [10]. To begin this process, the physical pair of lines and its corresponding equivalent network model are shown in Fig. 3 with the following network parameters:

$$N = \frac{1}{K} \tag{1}$$

$$Z_1 = \frac{Z}{\sqrt{1-K^2}} \tag{2}$$

$$Z_2 = Z\frac{\sqrt{1-K^2}}{K^2} \tag{3}$$

where

$$Z = \sqrt{Z_{\rm oe}Z_{\rm oo}} \tag{4}$$

and the coupling coefficient K is

$$K = \frac{Z_{\rm oe} - Z_{\rm oo}}{Z_{\rm oe} + Z_{\rm oo}}. \tag{5}$$

In (4) and (5), $Z_{\rm oe}$ and $Z_{\rm oo}$ are the even- and odd-mode impedances of the coupled lines, respectively. By substituting the network model for each of the coupled-line sections comprising the balun, the balun network of Fig. 4(a) is obtained. Further simplification of this prototype would require that the pair of transformers in parallel with the series stub Z_{oc3} be of identical turns ratio. This leads to the loss of one degree of freedom since the pair of coupled lines comprising the balun must now have the same coupling coefficient. Proceeding with this assumption results in Fig. 4(b) with N_a and N_b being of equal value N and the impedance of the series stub Z_{oc3} scaled up to $Z_{oc3} \cdot N^2$. Upon further simplification, the prototype of Fig. 4(c) can then be obtained after shifting the input transformer to the far right and absorbing it into the balanced load impedance. This is a redundant S-plane bandpass prototype with two zeros at $S = 0$, i.e., at dc, two zeros at infinity, and a redundant quarter-wave-long transmission line also known as a unit element (UE) [10]. Thus, given the impedances of the final prototype as shown in Fig. 4(d), the coupled-line parameters of the balun can then be extracted after solving the following equations:

$$Z_{c1} = \frac{Z_{2a}}{N^2} = Z_a\sqrt{1-K^2} \tag{6}$$

$$Z_{c2} = \frac{Z_{2b}}{N^2} = Z_b\sqrt{1-K^2} \tag{7}$$

$$Z_{c3} = \frac{Z_{1a} + Z_{1b}}{N^2} = (Z_a + Z_b)\frac{K^2}{\sqrt{1-K^2}}. \tag{8}$$

This gives the coupled-line parameters in terms of the prototype's circuit elements as follows:

$$K = \sqrt{\frac{Z_{c3}}{Z_{c1} + Z_{c2} + Z_{c3}}} \tag{9}$$

$$Z_a = \frac{Z_{c1}}{\sqrt{1-K^2}} \tag{10}$$

$$Z_b = \frac{Z_{c2}}{\sqrt{1-K^2}}. \tag{11}$$

Once K, Z_a, and Z_b are determined, the even- and odd-mode impedances of each individual coupled-line pair comprising the balun could then be found after solving (4) and (5) to give

$$Z_{\rm oea} = Z_a\sqrt{\frac{1+K_a}{1-K_a}} \text{ and } Z_{\rm ooa} = \frac{Z_a^2}{Z_{\rm oea}} \tag{12}$$

$$Z_{\rm oeb} = Z_b\sqrt{\frac{1+K_b}{1-K_b}} \text{ and } Z_{\rm oob} = \frac{Z_b^2}{Z_{\rm oeb}}. \tag{13}$$

Also, for further clarity, the coupling coefficients used in (12) and (13) are, as stated earlier, of identical values and defined using (5) as

$$K_a = \frac{Z_{\rm oea} - Z_{\rm ooa}}{Z_{\rm oea} + Z_{\rm ooa}} = K_b = \frac{Z_{\rm oeb} - Z_{\rm oob}}{Z_{\rm oeb} + Z_{\rm oob}} = K. \tag{14}$$

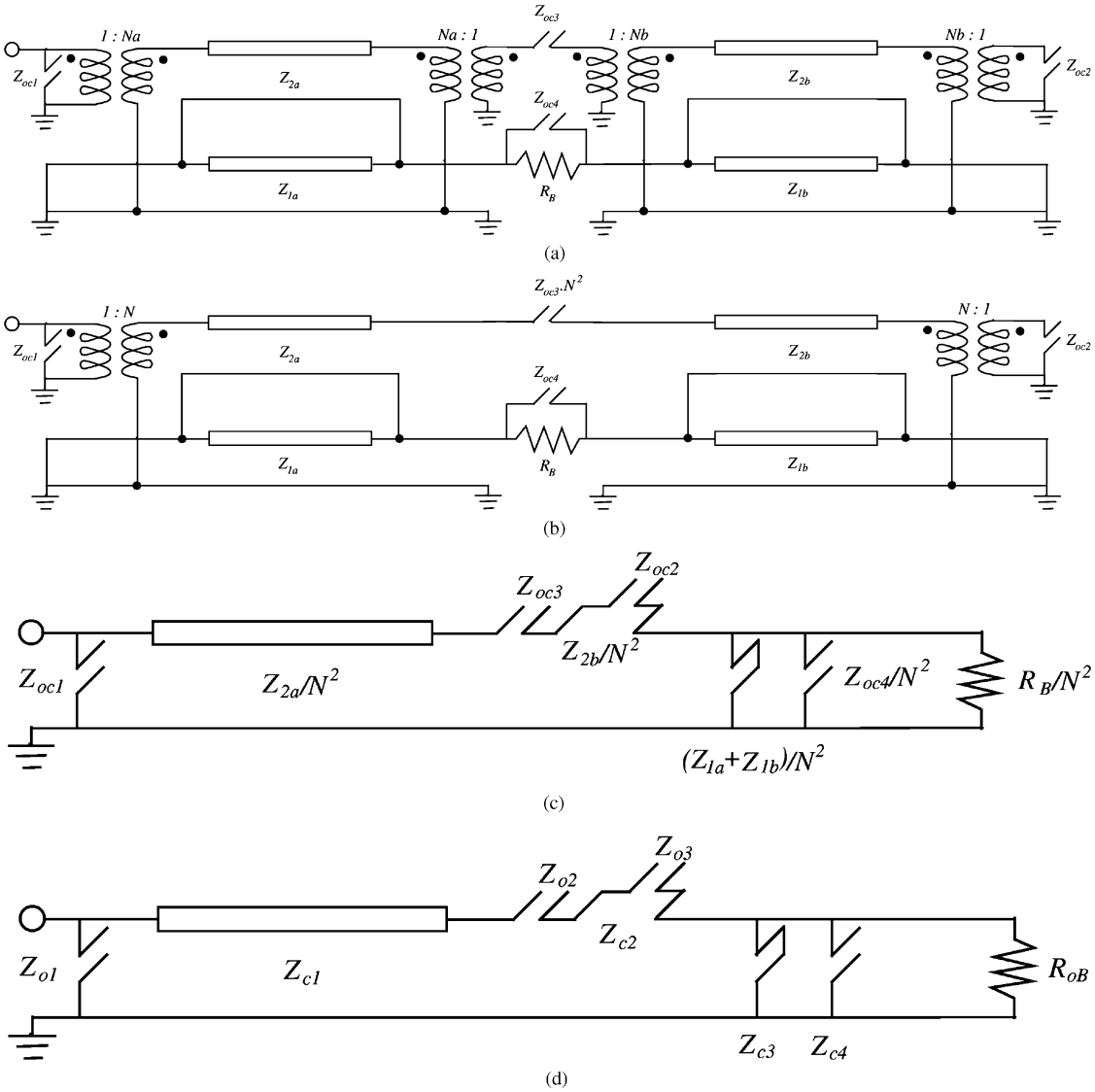

Fig. 4. Derivation of the S-plane bandpass prototype of the balun of Fig. 2. (a) After substitution of the network model of Fig. 3(b) for each pair of coupled lines. (b) After scaling up the series open-circuited stub, Z_{oc3} by N^2. (c) After shifting the input transformer throughout the network and absorbing it into the load resistance. (d) Final prototype.

Now the impedances of the open-circuited stub Z_{oc4} and the balanced load R_B can be found from

$$Z_{oc4} = \frac{Z_{c4}}{K^2} \tag{15}$$

$$R_B = \frac{R_{oB}}{K^2}. \tag{16}$$

Finally, without any further scaling, the impedances of the remaining stubs are found to be

$$\begin{aligned} Z_{oc1} &= Z_{o1} \\ Z_{oc2} &= Z_{o3} \\ Z_{oc3} &= Z_{o2}. \end{aligned} \tag{17}$$

Although this section developed synthesis equations based on a specific prototype corresponding to a bandpass balun topology, the procedure is general and is adaptable to other classes of baluns. Discussion of the new prototype classes will now commence. In this discussion, we will use the well-known circuit transformations shown in Fig. 5.

III. New S-Plane Bandpass Prototypes

A logical step in deriving miniaturized baluns is to apply the half-angle transform [12] to the synthesized S-plane highpass prototype [2], [3], [11] of Fig. 1. This transform is shown in Fig. 5(a) for an open-circuited stub. To elaborate on the mathematics involved in this transform, consider the impedance of an open-circuited stub [12]

$$\begin{aligned} Z_{oc} &= \frac{Z_o}{S} \\ &= -jZ_o \cot(\theta) \\ &= j\left(\frac{Z_o}{2}\right)\tan\left(\frac{\theta}{2}\right) - \frac{j\left(\frac{Z_o}{2}\right)}{\tan\left(\frac{\theta}{2}\right)} \end{aligned} \tag{18}$$

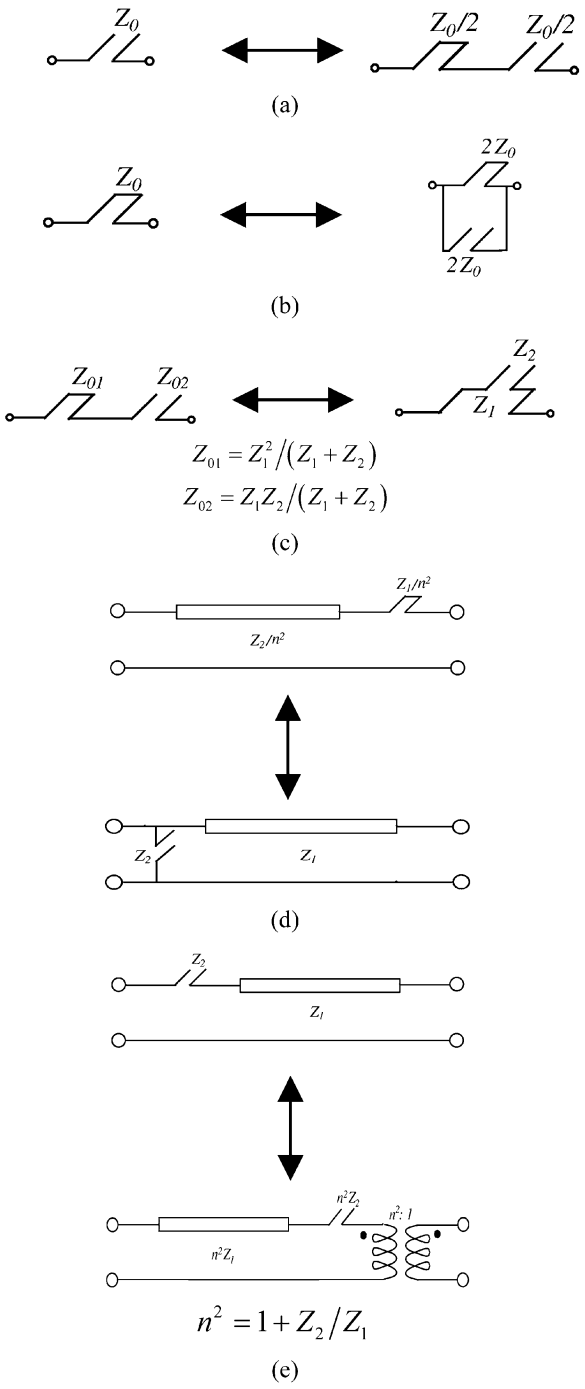

Fig. 5. Relevant circuit transformations. (a) Open- and (b) short-circuited stubs after application of the half-angle transform from [12]. (c) Equivalence between series connection of an open- and short-circuited stubs and stepped impedance transmission line from [10]. (d) First Kuroda transformation of a series short-circuited stub. (e) Second Kuroda transformation of a series open-circuited stub from [10].

where $\theta = (\pi/2)(f/f_o)$. It is clear that (18) is the series connection of short- and open-circuited stubs having characteristic impedances of $Z_o/2$ with half of the original electrical length. This implies that the resulting transmission-line resonators are a quarter wavelength long at $2f_o$, i.e., they are an eighth wavelength long at f_o. Through a similar analytical treatment, the short-circuited stub has the equivalence shown in Fig. 5(b). Application of this transform to the highpass prototype of Fig. 1 leads to the transformed prototype of Fig. 6(a) with the input UE now split into two equal pieces. The preceding step has not been previously utilized in papers concerning balun design. While the half-angle transformation does not affect the transmission characteristics of the network, it actually changes the transmission zero distribution of the prototype. Now the prototype possesses two zeros at dc, two zeros at infinity, and two nonredundant UEs, i.e., it is now a bandpass prototype with a commensurate frequency f_q which is $2f_o$. Thus, the balun equivalent of this prototype, shown in Fig. 6(b), is size reduced by almost a factor of two compared to a conventional balun design. However, the series open-circuited stub is difficult to realize in planar technology such as microstrip, and there is also scope for further size reduction if the open-circuited stubs are approximated by lumped capacitors. This is shown in Fig. 6(c). This prototype is therefore identified as Class A. In an attempt to derive other prototypes suitable for realization as Marchand balun structures, different sets of transmission zeros were tried, and various prototype networks were synthesized. Application of the classical synthesis technique in the transformed variable [13], [14] for an arbitrarily selected f_o, and f_q with specific sets of transmission zeros, results in the prototype Classes B and C shown in Figs. 7 and 8, respectively. In fact, Class-A prototypes may also be directly synthesized using the same technique [13], [14].

Subsequently, the synthesized network prototypes undergo several network transformations in the S-plane. This allows scaling of different elements of the prototype in order to obtain reasonably realizable even- and odd-mode impedances after using (9)–(11). These circuit transformations also lead to various balun topologies and allow flexible designs to be achieved. The essential circuit transformations are shown in Fig. 5; while many more transformations may be used, the scope of this paper is limited as summarized. As an example, transformed Class-B prototypes are presented in Fig. 9. Similar transformed Class-A prototypes may also be obtained in the same way.

Thus, the design strategy is to first classify the S-plane bandpass prototypes from a set of transmission zeros, apply circuit transformations, and then convert the specific prototypes to their physical balun realizations. The last step is performed by inspection in a backward manner as was done in Fig. 4. Subsequently, all of the open-circuited stubs loading the balun are then approximated by lumped capacitors at the center of the passband in the f-plane to obtain mixed lumped-distributed baluns. Section IV demonstrates this process using a step-by-step numerical example.

IV. A Numerical Example

A 50 : 100-Ω Class-B balun with a center frequency f_o of 1 GHz and a commensurate frequency f_q of 2 GHz is synthesized here. The objective is to design a balun with a return loss of >15 dB at the single-ended port and a bandwidth ratio of 1.54 : 1 giving lower and upper passband edge frequencies of

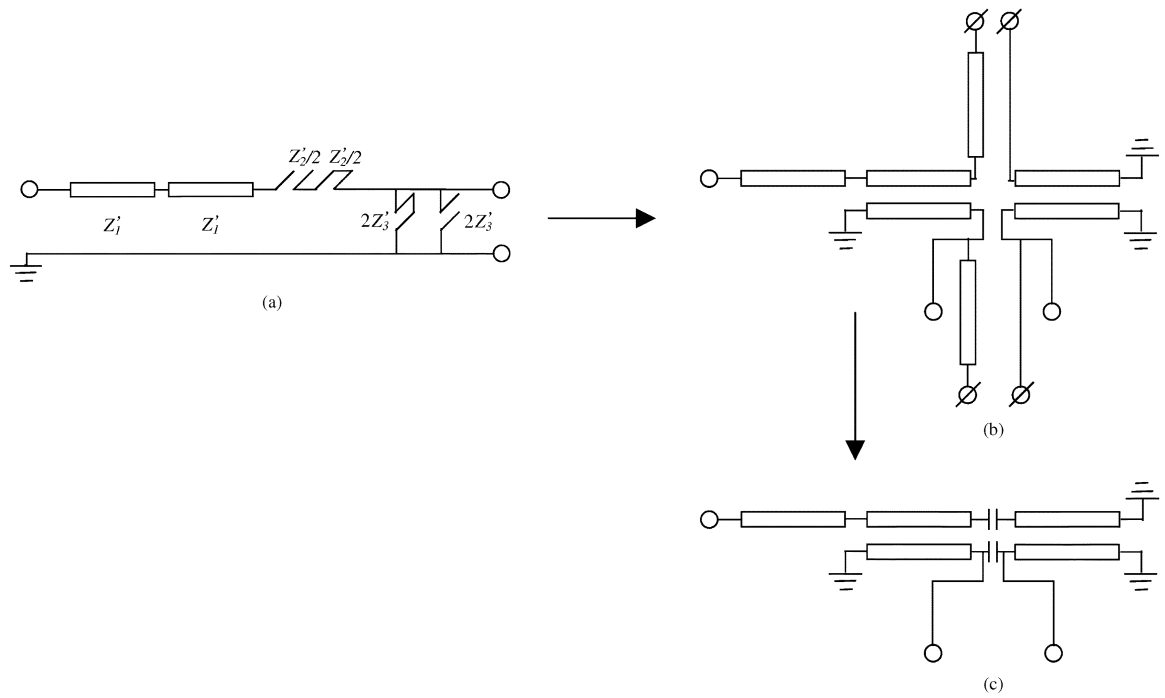

Fig. 6. Class-A balun. (a) Prototype derived by transforming the highpass prototype of Fig. 1(b) using the half-angle transformation. (b) Physical topology loaded with open-circuited stubs. (c) Miniaturized mixed lumped-distributed physical topology. (The distributed prototype has two zeros at dc, two zeros at infinity, and two nonredundant UEs.)

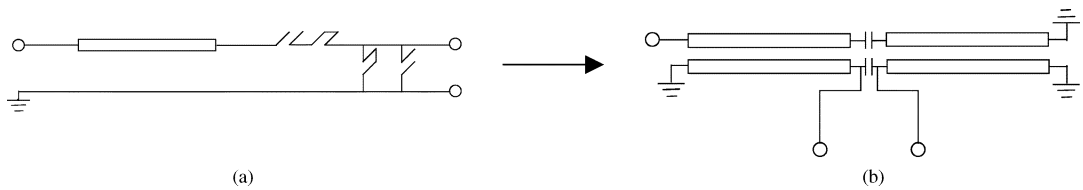

Fig. 7. Class-B balun. (a) Prototype with two zeros at dc, two zeros at infinity, and a redundant UE matching the single-ended source impedance. (b) Miniaturized mixed lumped-distributed physical topology.

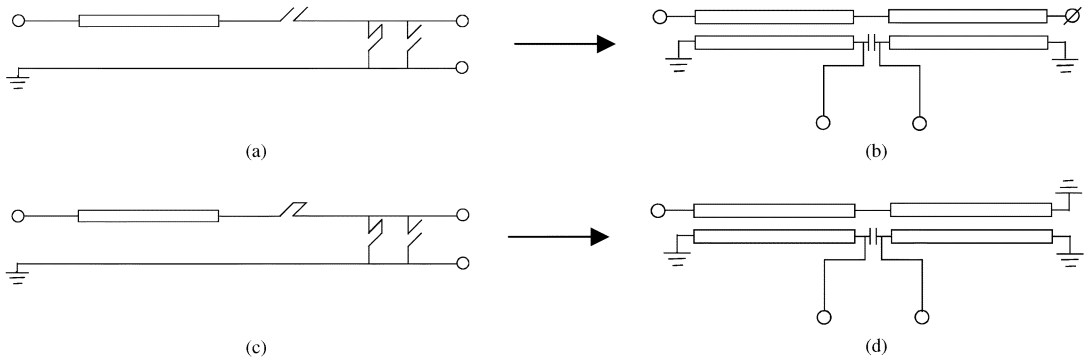

Fig. 8. Class-C baluns. (a) C1 prototype with two zeros at dc, a zero at infinity, and a nonredundant UE. (b) C2 prototype with a zero at dc, two zeros at infinity, and a nonredundant UE. (c) and (d) Corresponding miniaturized mixed lumped-distributed physical topologies.

0.82 and 1.26 GHz, respectively. The purpose is to implement the balun on an FR4 printed circuit board (PCB) with the following specification:

Substrate thickness: 62 mil (1.57 mm)
Relative dielectric constant: 4.7
Metal thickness: 2.2 mil (0.05 mm)
Minimum spacing: 7 mil (0.17 mm)
Loss tangent: 0.016. (19)

Now, the characteristic polynomial $K(S)$ of the prototype may be constructed for a passband ripple of 0.05 dB using [13] (or [14]) with two zeros at dc and two zeros at infinity leading to[1] (20), shown at the bottom of the following page, from which the square of the magnitude of the reflection transfer function is evaluated using

$$|S_{11}(S)|^2 = \frac{|K(S)|^2}{1+|K(S)|^2}. \tag{21}$$

[1]High precision of the numerical values must be retained throughout the synthesis process.

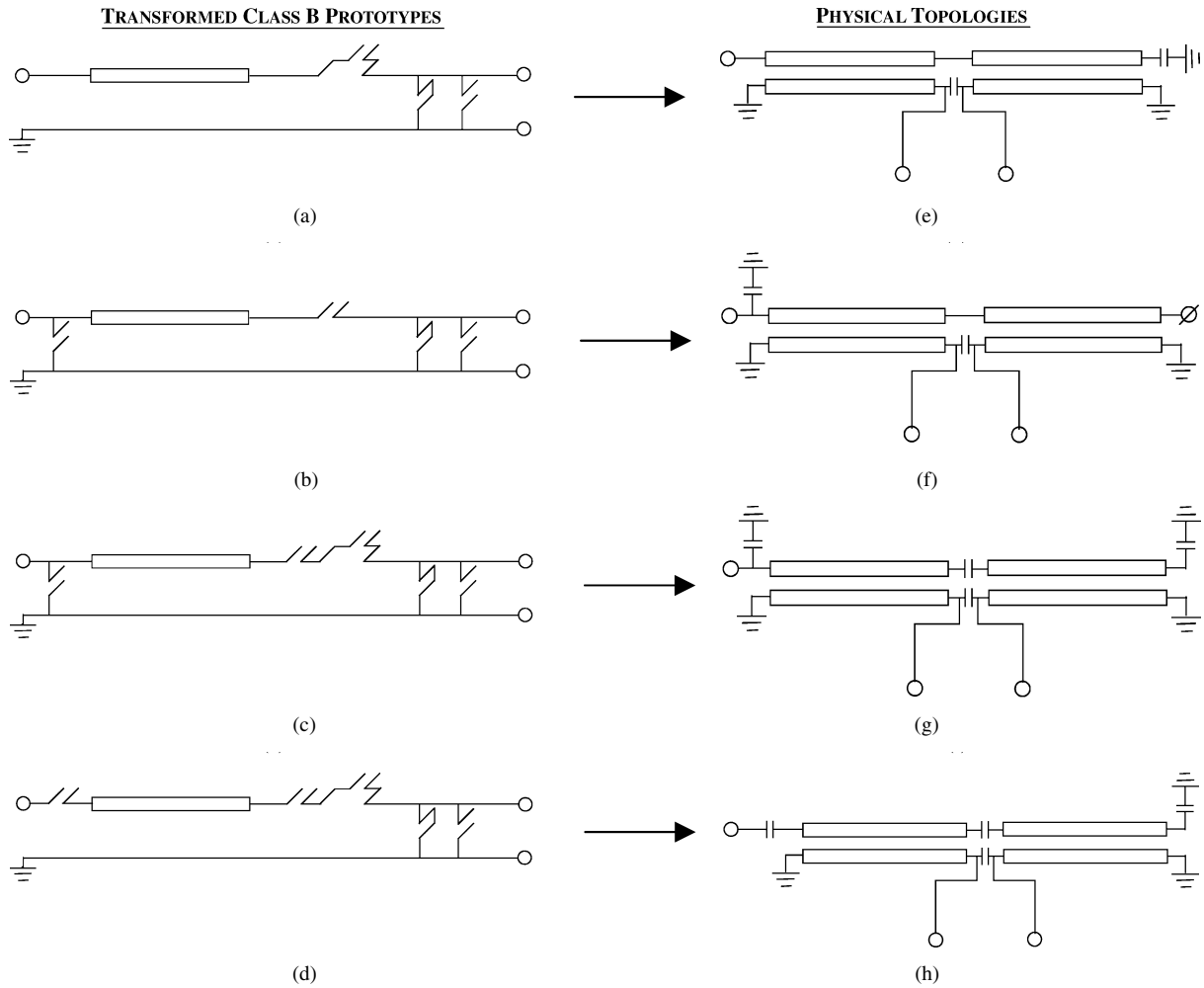

Fig. 9. Transformed Class-B prototypes of Fig. 7(a). (a) After application of the stepped impedance transmission line transformation to the series branch. (b) After application of the first Kuroda transformation. (c) After splitting the series connection of the open- and short-circuited stubs, application of the first Kuroda transformation to part of the series short-circuited stub and subsequently transforming the rest of the series branch to a stepped impedance transmission line. (d) After splitting the series connection of open- and short-circuited stubs, application of the second Kuroda transformation to part of the series open-circuited stub and subsequently transforming the rest of the series branch to a stepped impedance transmission line (and then absorbing the input transformer into the load impedance). (e)–(h) Corresponding miniaturized mixed lumped-distributed physical topologies.

$S_{11}(S)$ may then be found with the knowledge of

$$|S_{11}(S)|^2 = S_{11}(S) \cdot S_{11}(-S) \tag{22}$$

leading to (23), shown at the bottom of this page. The input impedance is then evaluated in a 1-Ω system from

$$Z_{\text{in}}(S) = \frac{1 + S_{11}(S)}{1 - S_{11}(S)} \tag{24}$$

which is then synthesized using standard element extraction. Upon synthesis, the resulting prototype is scaled up to suit a 50-Ω system, and a 50-Ω UE was then added after the source impedance, resulting in the prototype of Fig. 10(a). At this point, according to (6)–(8), we have the following circuit parameters obtained from Fig. 10(a):

$$\begin{aligned} Z_{c1} &= 50\ \Omega \\ Z_{c2} &= 44.863\ \Omega \\ Z_{c3} &= 60.434\ \Omega \end{aligned} \tag{25}$$

$$K(S) = \frac{(0.7232261254S^4 + 1.868909798S^2 + 0.9448913438)}{(2S^2)} \tag{20}$$

$$S_{11}(S) = \frac{(0.7232261254S^4 + 1.868909798S^2 + 0.9448913438)}{(0.7232261254S^4 + 1.611778003S^3 + 3.664909798S^2 + 1.842294719S + 0.9448913438)} \tag{23}$$

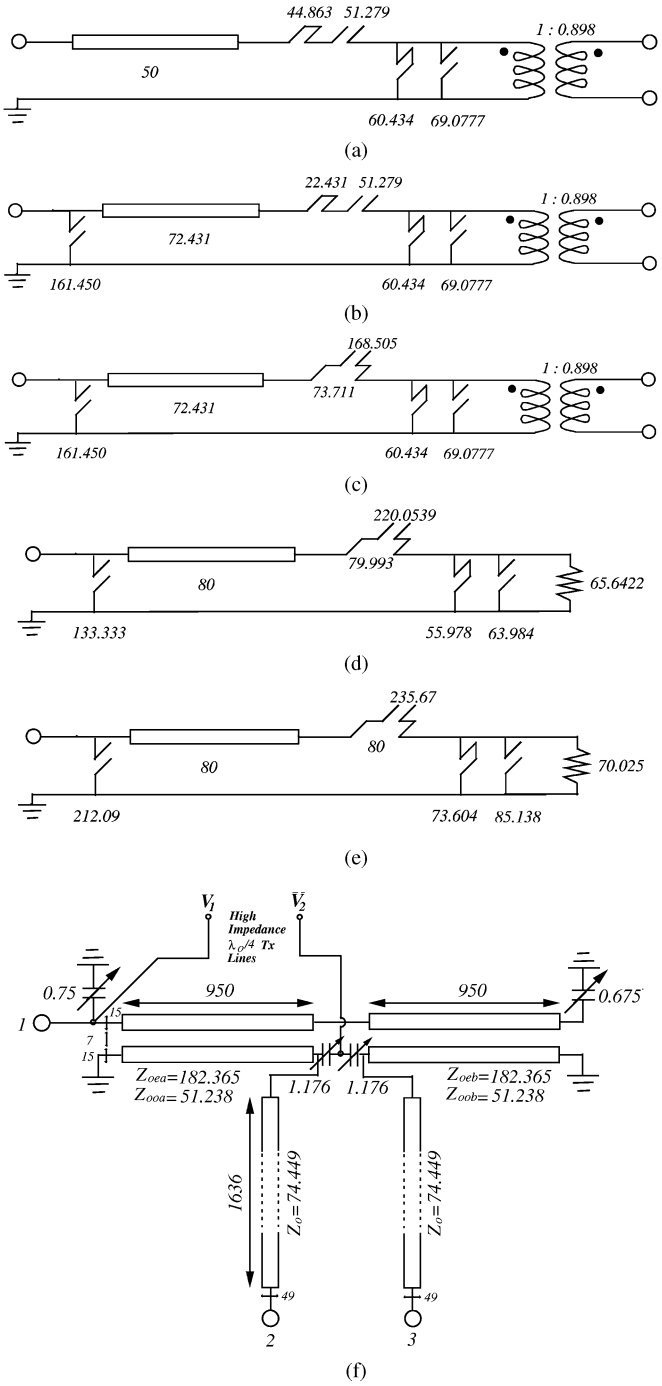

Fig. 10. Relevant transformations for a 50 : 100-Ω 1-GHz balun. (a) Class-B prototype with a passband ripple of 0.05 dB. (b) After equally splitting the series short-circuited stub and applying the first Kuroda transformation. (c) After transforming the series branch into a stepped impedance transmission line. (d) Resynthesized and retransformed Class-B prototype with a passband ripple of 0.0806 dB. (e) After some manual optimization applied to the prototype of (d) to obtain a return loss of approximately 20 dB. (f) Physical balun layout with lumped capacitors (in picofarads) and extra matching quarter-wavelength lines scaling the balanced load to 100 Ω. (dimensions are in mils).

and, thus, substituting (25) into (9)–(11) gives

$$\begin{aligned} K_a &= K_b = K = 0.624 \\ Z_a &= 63.974\ \Omega \\ Z_b &= 57.401\ \Omega. \end{aligned} \tag{26}$$

Now the parameters in (26) are then substituted in (12)–(13) to give

$$\begin{aligned} Z_{\mathrm{oea}} &= 132.915\ \Omega \\ Z_{\mathrm{ooa}} &= 30.792\ \Omega \end{aligned} \tag{27}$$

$$\begin{aligned} Z_{\mathrm{oeb}} &= 119.259\ \Omega \\ Z_{\mathrm{oob}} &= 27.628\ \Omega. \end{aligned} \tag{28}$$

Conversion of the above set of even- and odd-mode impedances into physical dimensions using ADS[2] yields width ϖ and spacing S of values

$$\begin{aligned} \varpi_1 &= 29.88\ \text{mil}\ (0.75\ \text{mm}) \\ S_1 &= 3.17\ \text{mil}\ (0.08\ \text{mm}) \end{aligned} \tag{29}$$

$$\begin{aligned} \varpi_2 &= 38.15\ \text{mil}\ (0.96\ \text{mm}) \\ S_2 &= 2.49\ \text{mil}\ (0.06\ \text{mm}). \end{aligned} \tag{30}$$

Unfortunately, according to (19), the spacing between the coupled lines violates the minimum spacing restriction imposed by the PCB manufacturer. This is when the circuit transformations become useful. By transforming the prototype of Fig. 10(a) to that of Fig. 10(b) and making use of the stepped impedance transmission-line equivalence, the transformed prototype of Fig. 10(c) results. Performing similar manipulation as above, we get new coupled-line parameters as follows:

$$\begin{aligned} Z_{\mathrm{oea}} &= 157.76\ \Omega \\ Z_{\mathrm{ooa}} &= 47\ \Omega \end{aligned} \tag{31}$$

$$\begin{aligned} Z_{\mathrm{oeb}} &= 160.548\ \Omega \\ Z_{\mathrm{oob}} &= 47.836\ \Omega. \end{aligned} \tag{32}$$

This leads to new physical dimensions of

$$\begin{aligned} \varpi_1 &= 17.14\ \text{mil}\ (0.43\ \text{mm}) \\ S_1 &= 8.79\ \text{mil}\ (0.22\ \text{mm}) \end{aligned} \tag{33}$$

$$\begin{aligned} \varpi_2 &= 16.16\ \text{mil}\ (0.41\ \text{mm}) \\ S_2 &= 9.01\ \text{mil}\ (0.22\ \text{mm}). \end{aligned} \tag{34}$$

It is now clear that the above dimensions are realizable; however, it is always desirable to obtain identical coupled-line parameters to construct a physically symmetrical balun structure. This would allow the division of the balanced load resistance by a factor of two to make feasible practical measurements. In terms of circuit synthesis, it is actually possible to obtain a prototype with elements values such that this condition is satisfied. This is done by iterating on the synthesis cycle for different values of passband ripple until the evaluated values of the resulting even- and odd-mode impedances of the pair of coupled lines become identical. Fig. 10(d) shows another synthesized and transformed prototype achieving a passband ripple of 0.0806 dB, i.e., a return loss of approximately 17.37 dB with the same bandwidth ratio of 1.54 : 1. It is now seen from the figure that the impedances of the UE and the input series stepped transmission line are virtually equal ($80 \approx 79.993\ \Omega$)—this is just the necessary required condition.

[2]Advanced Design System (ADS), Version 2003A, Agilent Technol., Palo Alto, CA, 2004.

Now, from Fig. 10(d), we have

$$Z_{c1} \cong Z_{c2} = 80\,\Omega$$
$$Z_{c3} = 55.978\,\Omega \tag{35}$$

and substituting these into (9)–(11) yields

$$K_a = K_b = K = 0.5091$$
$$Z_a = Z_b = 92.946\,\Omega. \tag{36}$$

Evaluating (12)–(13) using (36) gives identical coupled-line parameters of values

$$Z_{\mathrm{oea}} = Z_{\mathrm{oeb}} = 162.966\,\Omega$$
$$Z_{\mathrm{ooa}} = Z_{\mathrm{oob}} = 53.011\,\Omega. \tag{37}$$

At this stage, a manual optimization step is believed to improve the return loss level. Doing so results in the circuit of Fig. 10(e) with a return loss of approximately 20 dB. However, the values of the impedances of the UE and input-series stepped transmission line must remain fixed (80 Ω) to guarantee the condition of physical symmetry. The prototype of Fig. 10(e) results in the physical balun layout of Fig. 10(f) with even- and odd-mode impedances as shown in the same figure. In a similar step as before, ADS was utilized to obtain some physical dimensions that were found to be

$$\varpi_1 = \varpi_2 = 10.2 \text{ mil } (0.25 \text{ mm})$$
$$S_1 = S_2 = 9.08 \text{ mil } (0.23 \text{ mm}). \tag{38}$$

The shunt open-circuited stub at the balanced output and the balanced load R_B must now be scaled accordingly using (15) and (16) with K evaluated as 0.561 to give 270.51 and 221.707 Ω, respectively. The balanced load impedance is then scaled to 100 Ω by a pair of transmission lines of impedance 74.449 Ω each. The remaining stubs are left unscaled according to (17).

Due to the fact that we are using a bandpass prototype, it is possible to approximate any or all of its open-circuited stubs by lumped capacitors with very little deterioration of circuit's passband performance. Now, each open-circuited stub is approximated by a lumped capacitor using the relationship

$$j\left(\frac{1}{Z_i}\right) \cdot \tan\left(\frac{\pi}{2} \cdot \frac{f_o}{f_q}\right) = j2\pi f_o C_i \tag{39}$$

where Z_i is the impedance of the open-circuited stub and C_i its corresponding capacitor value. This approximation is valid over the vicinity of the passband of the filter but will affect the upper stopband characteristics. However, in many cases, such a step will lead to better stopband performance suppressing upper undesired passbands. This point will be elaborated upon in Section V. Performing the approximation using (39) gives values of capacitors as shown in Fig. 10(f). A final superficial optimization step is required to adjust the return loss level after approximation to lumped capacitors giving lines that are 15-mil (0.38 mm) wide, 7-mil (0.17 mm) apart, and 950-mil (24.13 mm) long. Also, each output matching line is 49-mil (1.24 mm) wide, and 1636-mil (41.55 mm) long.

It is interesting to note that this example shows yet another transformed Class-B balun topology not included in Fig. 9. This topology was also used in [5], apparently without any rationale behind its derivation.

V. Experimental Implementations and Results

A. Implementation of Class-B Balun

The layout of Fig. 10(f) (without the high-impedance transmission lines) was implemented and its measured and simulated performance, using high-quality lumped capacitors with Q of 600 are shown in Fig. 11. In Fig. 11(a) and (b), the measured mid-band insertion loss is about 3.6 dB. The excess 0.6 dB of loss is mainly attributed to substrate and conductor losses. The measured maximum amplitude error, from Fig. 11(c), is about 0.2 dB over the passband which is just slightly better than the simulation by about 0.05 dB. Fig. 11(d) shows a plot of transmission phase error over the passband, indicating a maximum measured phase error of approximately 2° at 1.2 GHz in contrast to approximately 4° according to simulation. It is fair to note at this point that the performance of the balun is excellent. The practical capacitor values used were 0.8, 0.7, and 0.6 pF, as opposed to the simulated values of [from Fig. 10(f)] 0.75, 0.675, and 0.588 pF, respectively. The differences are due to the microstrip vias that were assumed to be ideal in the simulation and as a result of adjusting the amplitude and phase responses to counteract the intrinsic difference between the even- and odd-mode phase lengths of the microstrip media.

A crucial point in the design of an efficient radio frequency (RF) system is the rejection of unwanted signals over a broad frequency range, and generally a synthesizable approach to circuit and system realization is desired. The new baluns introduced in this paper lend themselves to flexible designs since the design approach is based on bandpass prototypes with selection of the commensurate frequency f_q. Fig. 11(e) shows the simulated f-plane response of the circuits of Fig. 10(a)–(e), i.e., before the approximation of the open-circuited stubs by lumped capacitors. The first higher stopband is centered at f_q (2 GHz) while the following stopbands occur periodically at nf_q, where $n = 2, 3, 4, \ldots$. The second passband occurs at $2f_q - f_o$ also recurring periodically at $(2f_q - f_o) + m$, where $m = 2, 4, 6, \ldots$. However, also shown in Fig. 11(e) is the measured performance of the implemented balun, i.e., with all of the open-circuited stubs approximated by lumped capacitors. Now, it is clear that the approximation step benefits the stopband rejection of the balun since the second passband now occurs at about 4 GHz with wider stopband performance around 3 GHz. Thus, size reduction and control of the stopband performance are simultaneously made possible through the design approach based on bandpass prototypes.

B. Implementation of Class-B Tunable Balun

A second implementation of the above design was done with the objective of constructing an electronically tunable balun. This was another reason behind the choice of the specific sequence of circuit transformation used in Section V-A. It is generally known that passive circuits with wide bandwidths require strong coupling between their circuit elements. This is a problem particularly if the desired implementation requires coupled lines since the physical dimensions become unrealizable. A planar S-plane highpass balun is no exception [3]. A very attrac-

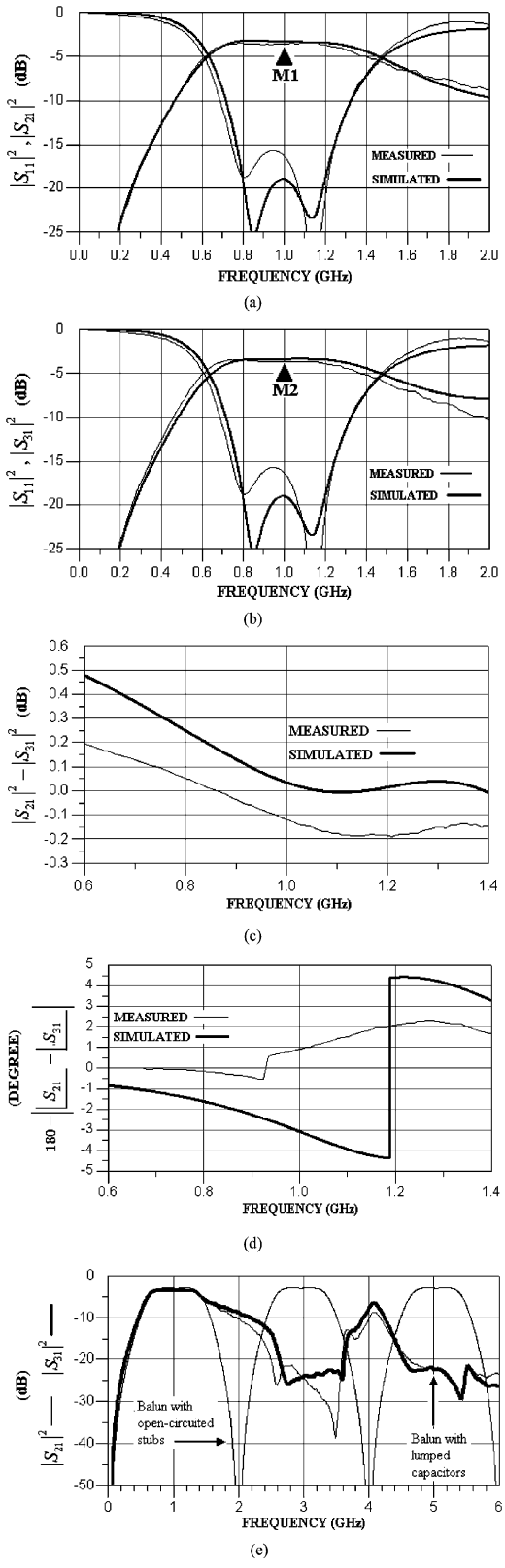

Fig. 11. Measured and simulated balun performance of Fig. 10(f) without bias lines and with high Q lumped capacitors. (a) $|S_{21}|^2$ and $|S_{11}|^2$ (M1: 1 GHz, -3.6 dB). (b) $|S_{31}|^2$ and $|S_{11}|^2$ (M2: 1 GHz, -3.5 dB). (c) Transmission coefficients amplitude error. (d) Transmission coefficients phase error. (e) Broad-band transmission coefficients.

tive feature of the S-plane bandpass balun presented here is the feasibility of tuning its passband using variable capacitors. This

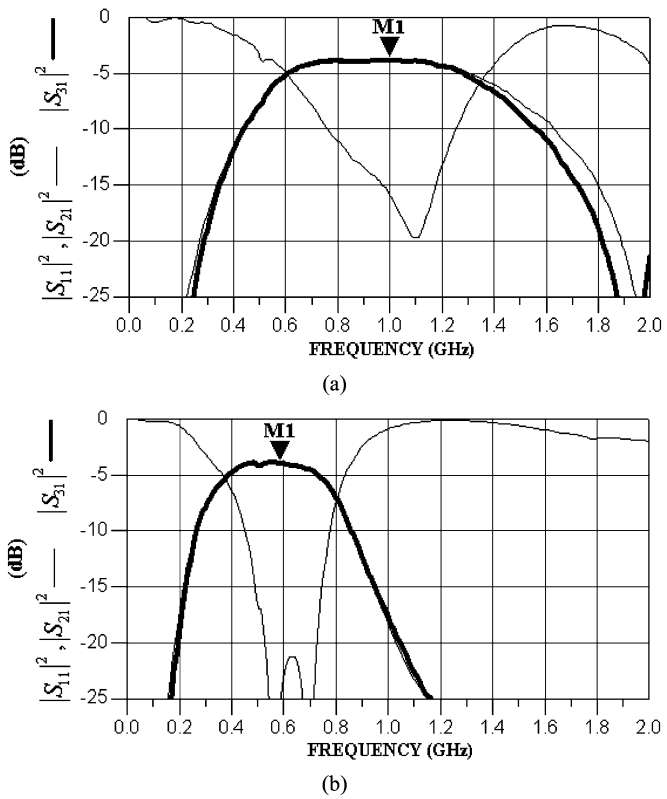

Fig. 12. Measured performance of tunable balun of Fig. 10(f) with bias lines and low Q varactor diodes in: (a) State 1 (M1: 1 GHz, -3.82 dB) and (b) State 2 (M1: 0.58 GHz, -4.04 dB).

implies that a moderate bandwidth balun may be designed and then tuned up/down in frequency to cover a wider bandwidth.

This was done using the layout of Fig. 10(f) with the pair of quarter-wavelength bias lines (at 1 GHz) connected to low-impedance voltage sources. Tunable capacitors with capacitance ratios of $10:1$[3] replaced the high Q lumped capacitors. The Q of the tunable capacitors was measured as roughly 12 at 1 GHz. This low Q has little effect on the in-band insertion loss due to the original design of the balun with a BR of $1.54:1$. The passband of the balun was tuned down from 1 GHz (State 1) to 0.58 GHz (State 2). This gives a sizable tuned frequency range of 1.7 (i.e., 1/0.58) with approximately $6:1$ capacitance ratios (see Fig. 12).

At 0.58 GHz, the Q of the varactor diodes naturally improves to about 30, but there will be extra reactances added to the balun structure at the biasing points due the limited bandwidth of the bias lines originally designed at 1 GHz. This contributed to some loss resulting in a measured mid-band IL at 0.58 GHz of 4.04 dB. Also, the measured maximum amplitude and phase errors in State 2 were 0.2 dB and 1°, respectively. At this stage, it is worth mentioning that a conventional design based on an S-plane highpass prototype would not have made tunability of the center frequency possible.

VI. Conclusion

New classes of baluns have been introduced based on an established exact synthesis technique that is widely used in filter

[3]Silicon tuning diodes, BB833, Infineon Technol., 2004.

design. The balun prototypes introduced here are synthesized from a specification of a set of transmission zeros with bandpass characteristics and possess various features such as small overall size and controlled broad stopband rejection. In many RF communications applications, the functions of filtering and balun transformations can now be realized by a single network, thus reducing the overall system losses compared to two separate realizations. The measured performance of an implemented Class-B balun agrees very well with the presented theory. Furthermore, by appropriate circuit transformations, Classes A and B can be made tunable. This was demonstrated with a Class-B tunable Marchand balun. This is the first tunable balun showing potential use in wide-band applications or in multifunctional RF/microwave systems covering various frequency bands.

REFERENCES

[1] N. Marchand, "Transmission line conversion transformers," *Electron.*, pp. 142–145, Dec. 1944.

[2] J. Cloete, "Graphs of circuit elements for the Marchand balun," *Microwave J.*, vol. 24, pp. 125–128, May 1981.

[3] C. L. Goldsmith, A. Kikel, and N. L. Wilkens, "Synthesis of Marchand baluns using multilayer microstrip structures," *Int. J. Microwave Millimeter-Wave Computer-Aided Eng.*, vol. 2, no. 3, pp. 179–188, 1992.

[4] B. J. Minnis and M. Healy, "New broadband balun structures for monolithic microwave integrated circuits," in *IEEE MTT-S Int. Microwave Symp. Dig.*, Jun. 1991, pp. 425–428.

[5] C. W. Tang and C. Y. Chang, "A semi-lumped balun fabricated by low temperature co-fired ceramic," in *IEEE MTT-S Int. Microwave Symp. Dig.*, Jun. 2002, pp. 2201–2204.

[6] K. S. Ang, Y. C. Leong, and C. H. Lee, "Analysis and design of miniaturized lumped-distributed impedance-transforming baluns," *IEEE Trans. Microw. Theory Tech.*, vol. 51, no. 3, pp. 1009–1017, Mar. 2003.

[7] A. M. Pavio and A. Kikel, "A monolithic or hybrid broad-band compensated balun," in *IEEE MTT-S Int. Microwave Symp. Dig.*, May 1990, pp. 483–486.

[8] K. Nishikawa, I. Toyoda, and T. Tokumitsu, "Compact and broad-band three-dimensional MMIC balun," *IEEE Trans. Microw. Theory Tech.*, vol. 47, no. 1, pp. 96–98, Jan. 1999.

[9] C. Tsai and K. C. Gupta, "A generalized model for coupled lines and its applications to two-layer planar circuits," *IEEE Trans. Microw. Theory Tech.*, vol. 40, no. 12, pp. 2190–2199, Dec. 1992.

[10] J. A. G. Malherbe, *Microwave Transmission Line Filters*. Norwell, MA: Artech House, 1979.

[11] M. Horton and R. Wenzel, "General theory and design of optimum quarter-wave TEM filters," *IEEE Trans. Microw. Theory Tech.*, vol. MTT-13, no. 5, pp. 316–327, May 1965.

[12] J. A. G. Malherbe, "Realization of elliptic function bandstop filters by means of resonated prototype," *IEEE Trans. Microw. Theory Tech.*, vol. MTT-25, no. 8, pp. 717–717, Aug. 1977.

[13] H. J. Orchard and G. C. Temes, "Filter design using transformed variable," *IEEE Trans. Circuit Theory*, vol. CT-15, no. 12, pp. 385–408, Dec. 1968.

[14] R. J. Wenzel, "Synthesis of combline and capacitively loaded interdigital bandpass filters of arbitrary bandwidth," *IEEE Trans. Microw. Theory Tech.* , vol. MTT-19, no. 8, pp. 678–686, Aug. 1971.

Wael M. Fathelbab (M'03) received the Bachelor of Engineering (B.Eng.) and Doctor of Philosophy (Ph.D.) degrees from the University of Bradford, Bradford, U.K., in 1995, and 1999 respectively.

From 1999 to 2001, he was an RF Engineer with Filtronic Comtek (U.K.) Ltd., where he was involved in the design and development of filters and multiplexers for various cellular base-station applications. He was subsequently involved with the design of novel RF front-end transceivers for the U.K. market with the Mobile Handset Division, NEC Technologies (U.K.) Ltd. He is currently a Research Associate with the Department of Electrical and Computer Engineering, North Carolina State University, Raleigh. His research interests include network filter theory, synthesis of passive and tunable microwave devices, and the design of broad-band matching circuits.

Michael B. Steer (S'76–M'82–SM'90–F'99) received the B.E. and Ph.D. degrees in electrical engineering from the University of Queensland, Brisbane, Australia, in 1976 and 1983, respectively.

He is currently a Professor with the Department of Electrical and Computer Engineering, North Carolina State University, Raleigh. In 1999 and 2000, he was a Professor with the School of Electronic and Electrical Engineering, The University of Leeds, where he held the Chair in microwave and millimeter-wave electronics. He was also Director of the Institute of Microwaves and Photonics, The University of Leeds. He has authored over 260 publications on topics related to RF, microwave and millimeter-wave systems, high-speed digital design, and RF and microwave design methodology and circuit simulation. He coauthored *Foundations of Interconnect and Microstrip Design* (New York: Wiley, 2000).

Prof. Steer is active in the IEEE Microwave Theory and Techniques Society (IEEE MTT-S). In 1997, he was secretary of the IEEE MTT-S. From 1998 to 2000, he was an elected member of its Administrative Committee. He is the Editor-in-Chief of the IEEE TRANSACTIONS ON MICROWAVE THEORY AND TECHNIQUES (2003–2006). He was a 1987 Presidential Young Investigator (USA). In 1994 and 1996, he was the recipient of the Bronze Medallion presented by the Army Research Office for "Outstanding Scientific Accomplishment." He was also the recipient of the 2003 Alcoa Foundation Distinguished Research Award presented by North Carolina State University.